Smart Structures and Systems, Vol. 1, No. 1 (2005) 83-101
DOI: http://dx.doi.org/10.12989/sss.2005.1.1.083

Modal identification and model updating of a reinforced concrete bridge

S. El-Borgi†, and S. Choura

Applied Mechanics and Systems Research Laboratory, Tunisia Polytechnic School, B.P. 743, La Marsa 2078, Tunisia

C. Ventura

Department of Civil Engineering, University of British Columbia, Vancouver, British Columbia, Canada

M. Baccouch and F. Cherif

Applied Mechanics and Systems Research Laboratory, Tunisia Polytechnic School, B.P. 743, La Marsa 2078, Tunisia

(Received October 23, 2003, Accepted July 27, 2004)

Abstract. This paper summarizes the application of a rational methodology for the structural assessment of older reinforced concrete Tunisian bridges. This methodology is based on ambient vibration measurement of the bridge, identification of the structure's modal signature and finite element model updating. The selected case study is the Boujnah bridge of the Tunis-Msaken Highway. This bridge is made of a continuous four-span simply supported reinforced concrete slab without girders resting on elastomeric bearings at each support. Ambient vibration tests were conducted on the bridge using a data acquisition system with nine force-balance accelerometers placed at selected locations of the bridge. The Enhanced Frequency Domain Decomposition technique was applied to extract the dynamic characteristics of the bridge. The finite element model was updated in order to obtain a reasonable correlation between experimental and numerical modal properties. For the model updating part of the study, the parameters selected for the updating process include the concrete modulus of elasticity, the elastic bearing stiffness and the foundation spring stiffnesses. The primary objective of the paper is to demonstrate the use of the Enhanced Frequency Domain Decomposition technique combined with model updating to provide data that could be used to assess the structural condition of the selected bridge. The application of the proposed methodology led to a relatively faithful linear elastic model of the bridge in its present condition.

Keywords: ambient vibration testing; output-only modal identification; enhanced frequency domain identification technique; finite element model updating.

1. Introduction

Tunisia has more than 3000 bridges with a minimum span length of 3 meters. Several of these bridges are old and were designed based on what today are considered outdated code regulations. A certain

†Associate Professor, Corresponding Author, E-mail: sami.elborgi@gnet.tn

number of these bridges have suffered load capacity degradation and damage due to traffic and environment. Current bridge inspection techniques are based on visual inspection techniques conducted by experienced engineers. A recent study conducted by the Federal Highways Administration Officials (Phares 2001) reported that at least 56% of visually based inspections of bridges in the United States were incorrect due to factors such as inspector's experience, bridge type and condition. Therefore, there is a need to develop rational and scientific methodologies for bridge inspection and evaluation (Catbas, *et al*. 2001).

This paper summarizes part of the ongoing work conducted in Tunisia within the framework of a research project funded by the Center for Testing and Construction Techniques which is affiliated with the Ministry of Infrastructure, Housing and Urban Planning. The project deals with the development of a rational methodology for the assessment of older reinforced concrete bridges. This methodology is based on the following steps: (a) response-only ambient vibration measurement of the bridge; (b) output-only modal signature identification of the bridge using the Enhanced Frequency Domain Decomposition technique; (c) finite element model updating which yields a linear elastic finite element model that reproduces as much as possible the real experimental behavior of the bridge; and (d) estimation of maximum bridge capacity and prediction of its failure modes based on detailed nonlinear finite element analyses. The focus of this paper is on the application of the first three steps of this methodology on the Boujnah bridge. The main objective of this study is to demonstrate the use of the Enhanced Frequency Domain Decomposition technique along with model updating to provide data that could be used to evaluate the structural condition of the Boujnah bridge.

(a) View from north to south

(b) View from west to east

Fig. 1 General view of the Boujnah bridge

2. Description of the case study

The tested bridge is located on the Tunis-Msaken highway, at about 18 km south of Tunis, the Capital of Tunisia with traffic going underneath. This bridge, shown in Fig. 1, was constructed in 1978 and consists of (i) a continuous four-span reinforced concrete slab resting on elastomeric bearings at each support; (ii) three intermediate piers each with a strip footing; and (iii) two abutments. The bridge was designed based on the allowable stress design method according to the French code CCBA68 (1968).

A longitudinal cross-section and plan view of the bridge are shown, respectively, in Figs. 2 and 3. The outside spans have a length of 8.75 meters and the inside spans have a length 16.75 meters. A typical cross-section of the continuous reinforced concrete slab is shown in Fig. 4. Two types of elastomeric bearings were used in the bridge, namely, type A for the pile supports and type B for the abutment supports. The dimensions of the elastomeric bearings are depicted in Fig. 5. A visual inspection of the bridge reveals no clear damage, mainly since it has been subjected over the years to minor traffic loading.

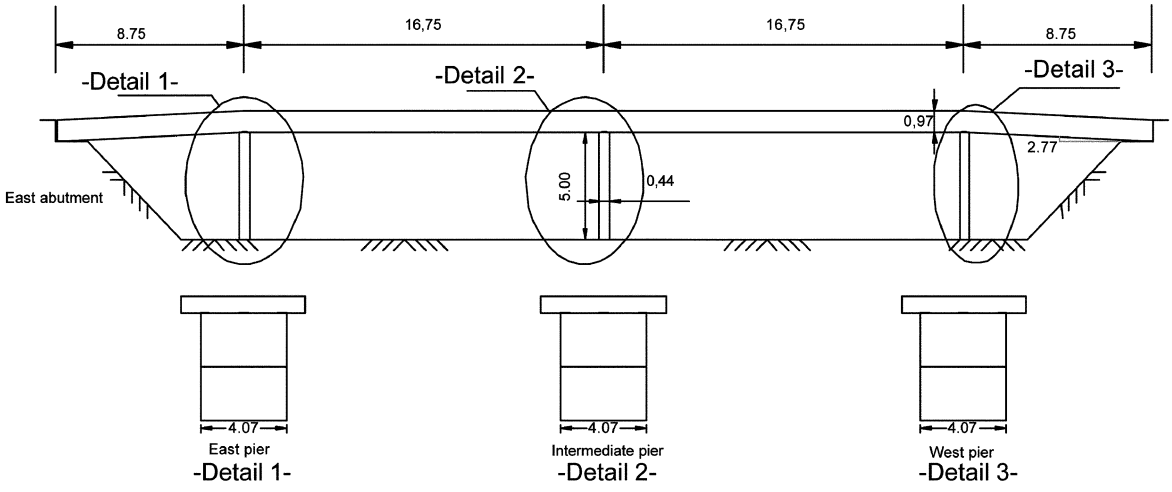

Fig. 2 Longitudinal cross-section of the bridge (dimensions in meters)

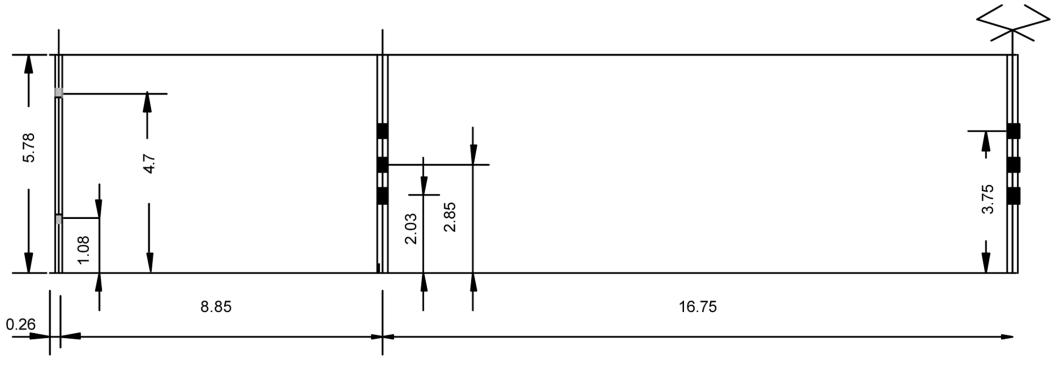

Fig. 3 Plan view of the bridge and distribution of the elastomeric bearings; Type A and type B supports are shown, respectively, in black and red (dimensions in meters)

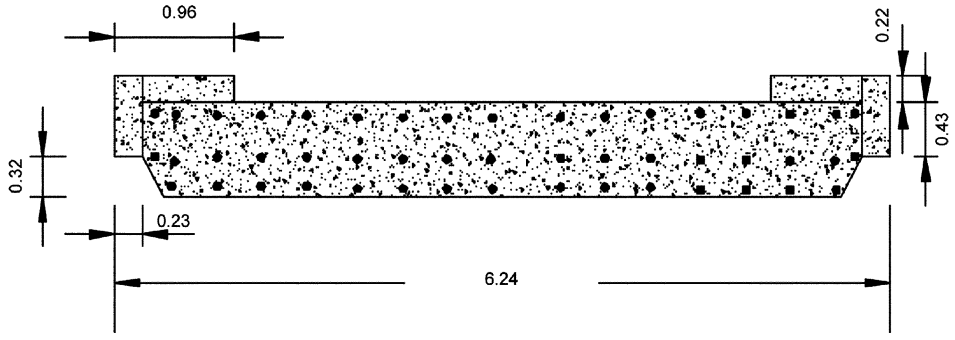

Fig. 4 Typical cross-section of the reinforced concrete continuous slab (dimensions in meters)

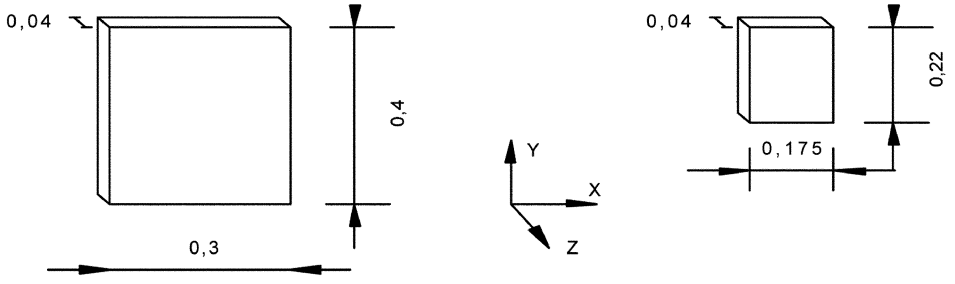

(a) Type A bearing (b) Type B bearing

Fig. 5 Dimensions of the elastomeric bearings (dimensions in meters)

3. Finite element modeling

A three dimensional detailed finite element model of the bridge was created using the commercially available SAP2000 computer program (Computers and Structures 2000). Four-noded shell elements were used to model the concrete slab and the piles, while the elastomeric bearings were modelled by linear elastic spring elements. The model, shown in Fig. 6, uses a total of 712 elements and 825 nodes. The x, y and z-coordinates represent, respectively, the longitudinal axis along the bridge, the horizontal transversal axis and the vertical axis (Fig. 6). The material behavior is assumed to be linear elastic, isotropic and homogeneous. The concrete modulus of elasticity was estimated at 32000 MPa based on concrete sample compression tests. The mass density of concrete was assumed to be 2500 kg/m^3. The stiffnesses of the elastomeric bearings, indicated in Table 1, were estimated based on an instantaneous modulus of elasticity of 4.8 MPa and an instantaneous shear modulus of 1.6 MPa.

The boundary conditions between the piers and the foundation were modelled by three uniaxial springs oriented, respectively, in the x, y and z-directions and attached to the bottom end of each pier along each node. The stiffness of these foundation springs was assumed to be equal to 10^{30} N/m representing the stiff soil conditions of the bridge site. The boundary conditions between the abutment and the bearing supports at both ends of the bridge were modelled as pinned supports along each node. The parameters selected for the finite element updating include the concrete modulus of elasticity, the elastomeric bearing stiffnesses and the foundation spring stiffnesses.

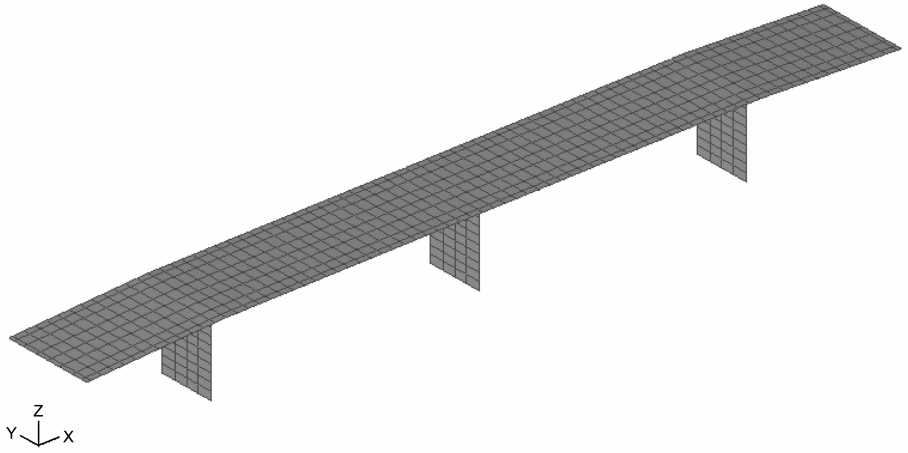

Fig. 6 Isometric view of the finite element model of the bridge

Table 1 Stiffnesses of the elastomeric bearings

	Elastomeric bearing stiffness		
	Kx	*Ky*	*Kz*
Bearing Type A	4.8×10^6 N/m	4.8×10^6 N/m	14.4×10^6 N/m
Bearing Type B	1.54×10^6 N/m	1.54×10^6 N/m	4.62×10^6 N/m

4. Ambient vibration testing and modal identification

For large structures, ambient vibration tests with output-only measurements are preferred over forced vibration tests where both the excitation and the response are measured. In ambient vibration testing, the measured response is representative of the actual operating conditions of the structure which vibrates due to natural excitation loads such as wind, microtremors, traffic and human activity. The fundamental assumption of the analysis of these ambient vibrations is that the inputs causing motion have white noise characteristics in the frequency range of interest. This assumption implies that the input loads are not driving the system at any particular frequency and therefore any identified frequency associated with significant strong response reflects structural modal response. However, in reality, some of the ambient disturbances, such as, for instance, an adjacent machine operating at a particular frequency may drive the structure at that frequency. In this case, the deformed shapes of the structure at such driving frequencies are called Operational Modes. This means that a crucial requirement of methods to analyze ambient vibration data is the ability to distinguish the natural structural modes from any imposed operational modes.

4.1. Description of the vibration equipment

Ambient vibration tests were conducted on the bridge using a sixteen-channel data acquisition system (Vibration Survey System Model VSS-3000, Kinemetrics, 1997) with nine force-balance uniaxial accelerometers (model FBA-ES-U, Kinemetrics, 2000). Photographs of the data acquisition and measurement equipment are shown in Fig. 7.

The sensors, which are capable of measuring accelerations of up to ±0.25 g with a resolution of

Fig. 7 Data acquisition system and an example of accelerometer attached to the bridge

0.1 μg, converted the physical excitation into electrical signals. Each accelerometer was connected to the data acquisition system using a 100 m long cable. Cables were used to transmit the electronic signals from sensors to the signal conditioner. The signal conditioner unit was used to improve the quality of the signals by removing undesired frequency contents (filtering) and amplifying the signals. The amplified and filtered analog signals were converted to digital data using an 16-bit resolution analog to digital converter (DaqBook/216 by Iotech Inc.) at a speed of 1000 kHz prior to storing on the data acquisition computer. The analog to digital converter was controlled by a data acquisition computer using a custom program called DasyLab version 5.6 by National Instruments (FEMTools Program Overview 2004). The analog to digital converter is capable of sampling up to sixteen channels at sampling frequencies between 0.2 Hz and 2000 Hz. Vibration experiments were conducted at a sampling frequency of 100 Hz with all channels set for a low-pass filter of 40 Hz. Signals converted to digital form were stored on the hard disk of the data acquisition computer in ASCII form.

4.2. Optimum sensor location

The developed finite element model was transferred to the commercial program FEMTools (2004) which was then used to simulate the experiments based on pre-defined locations and directions of the accelerometers. FEMTools, essentially, reduces the finite element model, shown in Fig. 6, into a pre-test model based on a small number of simulated sensor locations. The program then computes the frequencies and mode shapes based on this simplified model. The resulting mode shapes are called Simulated Experimental Mode Shapes (SEMS). In addition, FEMTools computes the frequencies and mode shapes of the complete finite element model shown in Fig. 6. The resulting mode shapes, called Finite Element Mode Shapes (FEMS), are then compared with the Simulated Experimental Mode Shapes in order to determine the effectiveness of the proposed sensor locations to capture the important dynamic properties of the structure. The correlation between the FEMS and SEMS modes can be quantified using the Modal Assurance Criterion (MAC) (Allemang and Brown 1982). A MAC value of 100% means perfect correlation between two vectors, while a 0% value means that the two vectors are completely uncorrelated.

FEMTools allows the user to create “maps” of zones of the structure sensitive to vibrations, as shown in Fig. 8. The red and blue colors in the scale shown in this figure indicate, respectively, the zones of maximum and minimum (or no) vibration in the structure. This information can be used to select the

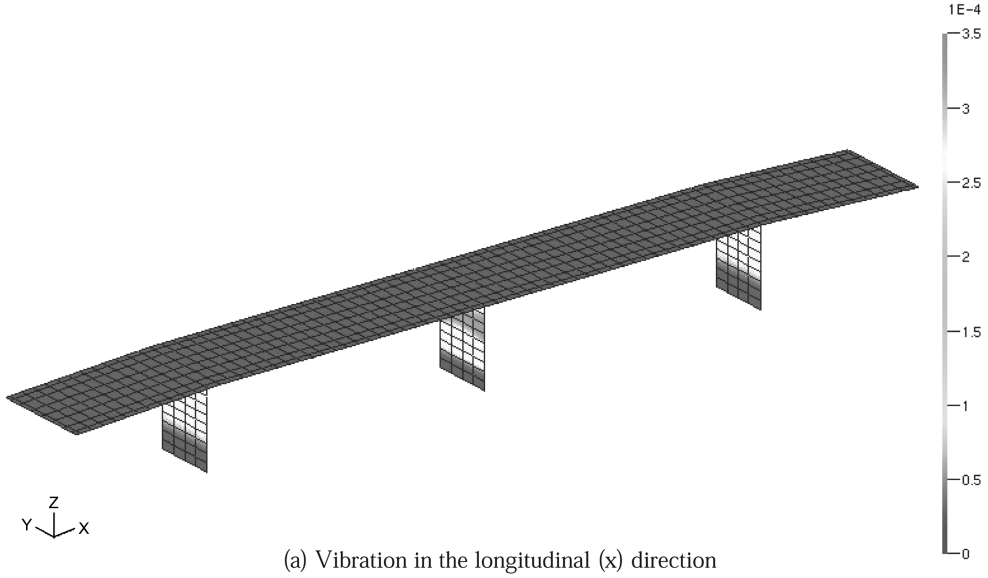

(a) Vibration in the longitudinal (x) direction

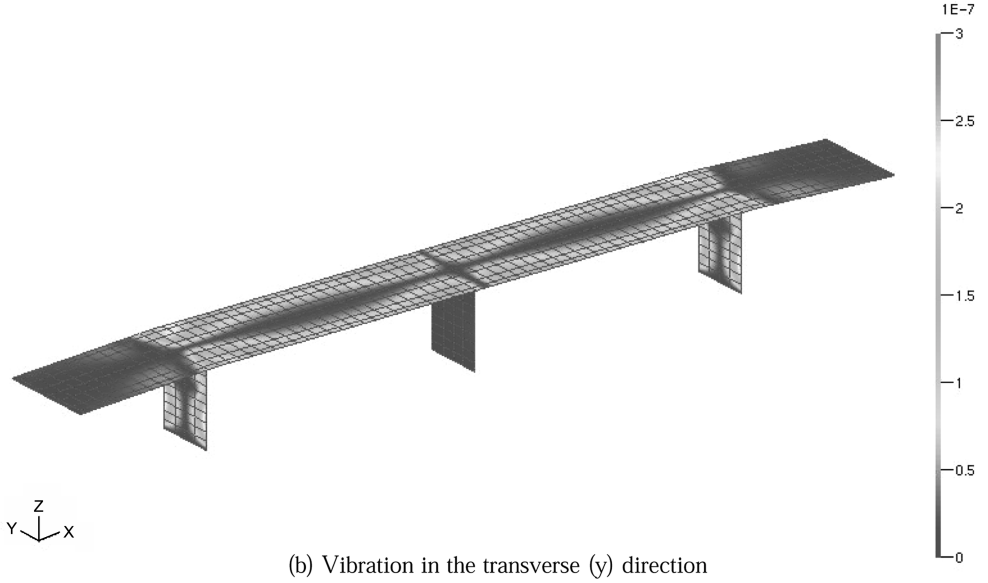

(b) Vibration in the transverse (y) direction

Fig. 8 Vibration-sensitive zones in the bridge

optimal locations where the measuring instruments can be installed. Based on the vibration-sensitive zones shown in Fig. 8, it was decided to have 40 measurement points on the slab and 9 measurements points at each of the east and west piers. The center pier was not instrumented because its access was quite dangerous (see Fig. 1) and the traffic along the highway could not be stopped to access this location. Based on this sensor configuration, shown in Fig. 9, the MAC values between the finite element mode shapes (FEMS) and the simulated experimental mode shapes (SEMS) are reported in Table 2. As depicted in this table, the diagonal terms are 100% and the off-diagonal terms are almost zero indicating perfect correlation.

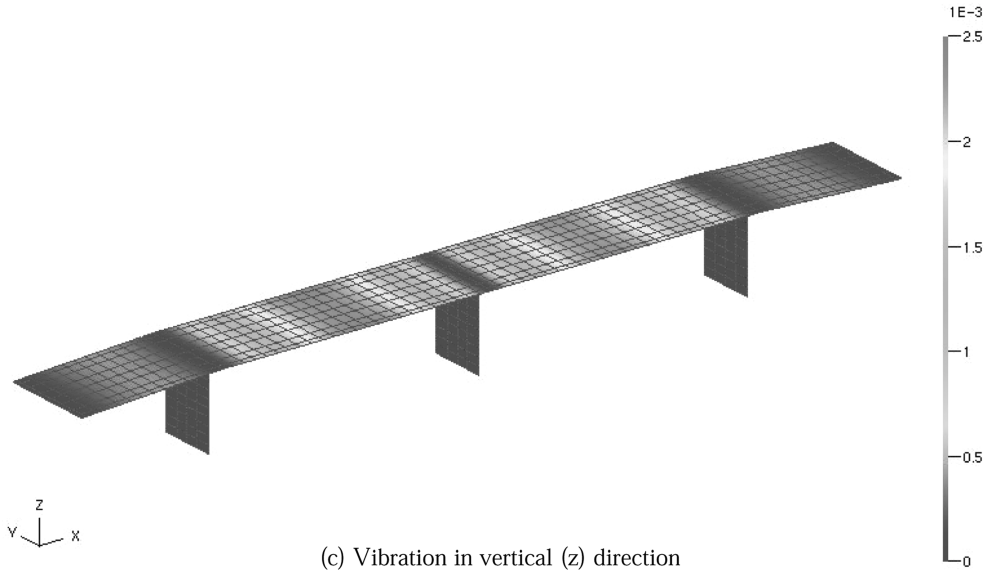

(c) Vibration in vertical (z) direction

Fig. 8 Continued

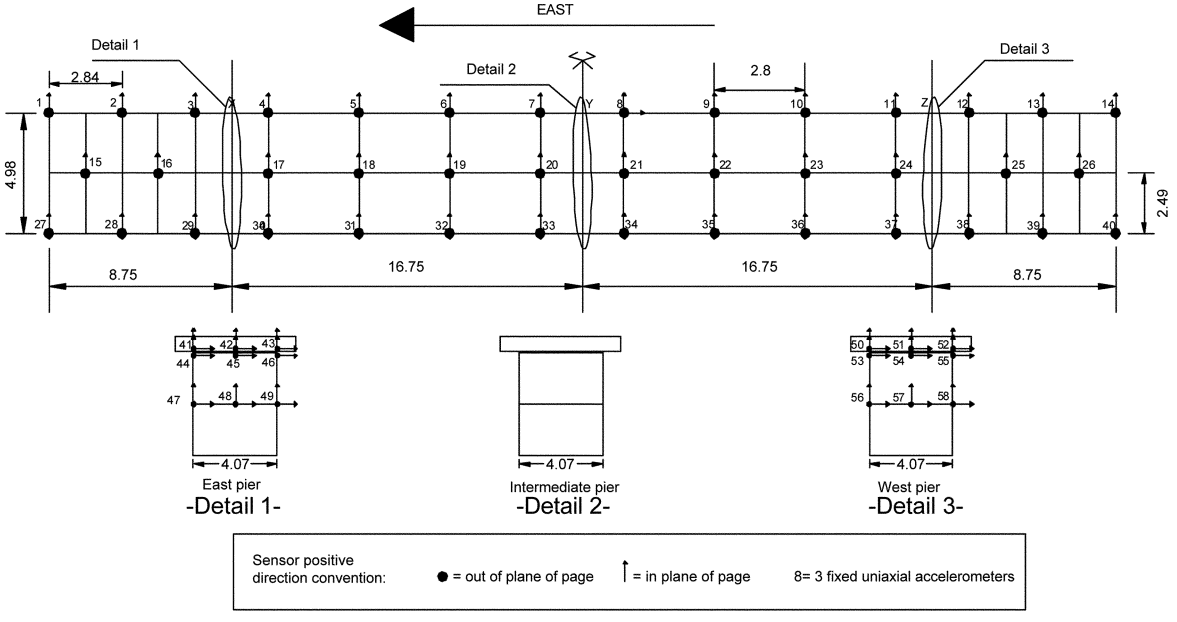

Fig. 9 Sensor locations and directions across the bridge (shown in dark circles)

4.3. Planning of the test setups

Fig. 8 shows that the vibrations were more dominant in the vertical (z) direction, followed by the transverse (y) direction for the case of the slab, while the vibrations in the piers were mostly in the x-

Table 2 MAC values between the finite element mode shapes and the simulated experimental mode shapes (in percentage)

Simulated Experimental Mode Shapes (SEMS)	Finite element mode shapes(FEMS)														
	1	2	3	4	5	6	7	8	9	10	11	12	13	14	15
1	**100.00**	0.00	0.00	0.00	0.00	0.00	0.00	0.00	0.00	0.00	0.00	0.00	0.00	0.00	0.90
2	0.00	**100.00**	0.00	0.00	0.00	0.00	0.00	0.00	0.00	0.00	0.00	0.00	0.00	0.00	0.00
3	0.00	0.00	**100.00**	0.00	0.00	0.00	0.00	0.00	0.00	0.00	0.00	0.00	0.00	0.00	0.00
4	0.00	0.00	0.00	**100.00**	0.00	0.00	0.00	0.00	0.00	0.00	0.00	0.00	0.00	0.00	0.00
5	0.00	0.00	0.00	2.60	**100.00**	0.00	0.00	0.00	0.00	0.00	0.00	0.00	0.00	0.00	0.00
6	0.00	0.00	0.00	0.00	0.00	**100.00**	0.00	0.00	0.00	0.00	0.00	0.00	0.00	0.00	0.00
7	0.00	0.00	0.00	0.00	0.00	0.00	**100.00**	0.00	0.00	0.00	0.00	0.00	0.00	0.00	0.40
8	0.00	0.00	0.00	0.00	0.00	0.20	0.00	**100.00**	0.00	0.00	0.00	0.00	0.00	0.00	0.00
9	0.00	0.00	0.00	0.00	0.00	0.00	0.00	0.00	**100.00**	0.40	0.60	0.00	0.00	0.00	0.00
10	0.00	0.00	0.00	0.00	0.00	0.00	0.00	0.00	0.40	**100.00**	0.00	0.70	0.00	0.00	0.00
11	0.00	0.00	0.00	0.00	0.00	0.00	0.00	0.00	0.60	0.00	**100.00**	0.50	0.00	0.00	0.00
12	0.00	0.00	0.00	0.00	0.00	0.00	0.00	0.00	0.00	0.70	0.50	**100.00**	0.10	0.00	0.00
13	0.00	0.00	0.00	0.00	0.00	0.00	0.00	0.00	0.00	0.00	0.00	0.10	**100.00**	0.10	0.00
14	0.00	0.00	0.00	0.00	0.00	0.00	0.00	0.00	0.00	0.00	0.00	0.30	0.10	**100.00**	0.00
15	0.00	0.00	0.00	0.00	0.00	0.00	0.00	0.00	0.00	0.00	0.00	0.00	0.00	0.00	**100.00**

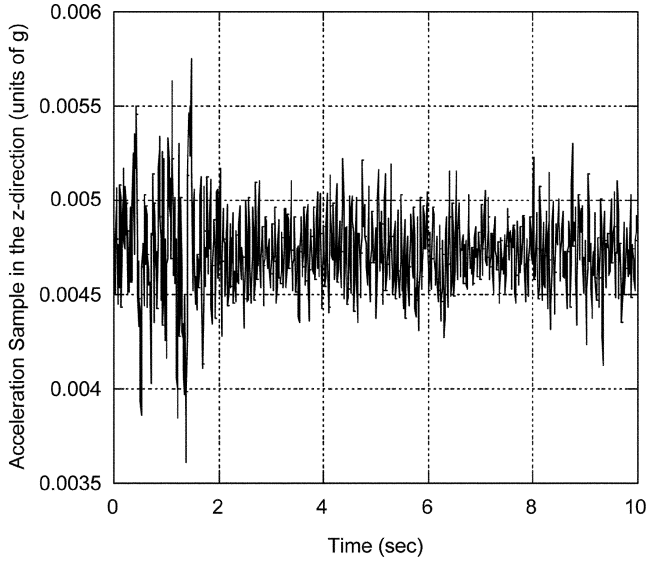

Fig. 10 Sample of acceleration measurement in the *z*-direction

direction, although small. As a result, the *y* and the *z*-components of the acceleration were measured at each point on the slab, while the *x*, *y* and *z*-components of the acceleration were measured at each point on the east and west piers.

Because the number of accelerometers and the number of channels was less than the number of measurements, the vibration measurement campaign was divided into 25 test setups, each lasting 10 minutes with a sampling frequency of 100 Hz. Each setup consisted of reference accelerometers which remained in their position throughout the campaign and the remaining sensors were moved to cover all

the measurement points. As shown in Fig. 9, three reference sensors were placed at measurement point No. 8 on the slab, selected in the zone of maximum vibration (Fig. 8c) to measure the acceleration in the x, y and z directions. The remaining measurement points, where the roving sensors were placed, as shown in Fig. 9. A sample of acceleration measurement in the z-direction is shown in Fig. 10.

4.4. Modal signature identification

The complex non-stationary nature of the unmeasured excitation requires the use of robust output-only modal identification techniques such as the Enhanced Frequency Domain Decomposition method (Brincker and Andersen 2000, Van Overschee and Moor 1996) and the Stochastic Subspace Identification methods (Brincker, *et al*. 2000). These methods were recently applied successfully to buildings and bridges (Brinker and Andersen 2000, Brincker, *et al*. 2000). These techniques are available in the program ARTeMIS (2004). In the present study, the Enhanced Frequency Domain Decomposition (EFDD) technique, which is a refinement of the Frequency Domain Decomposition (FDD) technique, was applied to extract the modal signature of the bridge.

4.4.1. Description of the FDD and EFDD techniques

The essence of the FDD technique is to perform an approximate decomposition of the measured system response into a set of responses of independent single degree of freedom (SDOF) systems, one for each mode. The decomposition is performed by a Singular Value Decomposition (SVD) of each of the spectral density matrices obtained from the measurements. The results of the decomposition are a set of singular values and associated singular vectors. The singular values are estimates of the auto spectral density of the component SDOF systems, and the singular vectors are estimates of the mode shapes.

The FDD technique involves the following main steps: (a) estimate spectral density matrices from the measured time series data; (b) perform a singular value decomposition of the spectral density matrices; (c) if multiple data sets are available, average the singular values from all data sets and display the results in graphical form; (d) scan the curves of singular values to "peak pick" the frequencies of interest and estimate the corresponding mode shapes at each frequency of interest using the information contained in the singular vectors of the SVD.

A further refinement of the FDD, the Enhanced Frequency Domain Decomposition (EFDD) method in ARTeMIS, uses the modal estimates from the FDD technique to identify the bell-shaped spectral functions of the SDOFs. From these functions, it estimates additional modal parameters such as modal damping.

4.4.2. Theory of the FDD and EFDD techniques

In the following paragraphs, both the FDD and the EFDD techniques are briefly summarized. The relationship between the unknown input $x(t)$ and the measured response $y(t)$ can be expressed as

$$G_{yy}(j\omega) = \overline{H}(j\omega)G_{xx}(j\omega)H(j\omega)^{T} \tag{1}$$

where $G_{xx}(j\omega)$ is the $r\times r$ Power Spectral Density (PSD) matrix of the input, r is the number of inputs, $G_{yy}(j\omega)$ is the $m\times m$ PSD matrix of the responses, m is the number of responses, $H(j\omega)$ is $m\times r$ Frequency Response Function (FRF) matrix, and "–" and the superscript T denote the complex

conjugate and matrix transpose, respectively. The FRF can be written in partial fraction; i.e., the pole/residue form:

$$H(j\omega) = \sum_{k=1}^{n}\left(\frac{R_k}{j\omega-\lambda_k}+\frac{\bar{R}_k}{j\omega-\bar{\lambda}_k}\right) \tag{2}$$

where n is the number of modes, λ_k is the pole and R_k is the residue:

$$R_k = \Phi_k \gamma_k^T \tag{3}$$

in which Φ_k and γ_k^T are the mode shape vector and the modal participation vector, respectively. Suppose the input is white noise; i.e., its PSD is a constant matrix.

Thus, $G_{xx}(j\omega) = C$ and Eq. (1) becomes:

$$G_{yy}(j\omega) = \sum_{k=1}^{n}\sum_{s=1}^{n}\left[\frac{R_k}{j\omega-\lambda_k}+\frac{\bar{R}_k}{j\omega-\bar{\lambda}_k}\right]C\left[\frac{R_s}{j\omega-\lambda_s}+\frac{\bar{R}_s}{j\omega-\bar{\lambda}_s}\right]^H \tag{4}$$

where superscript H denotes simultaneous complex conjugate and matrix transpose.

Multiplying the two partial fraction and making use of the Heaviside partial fraction theorem, after some mathematical manipulations, the output PSD can be reduced to a pole/residue form as follows:

$$G_{yy}(j\omega) = \sum_{k=1}^{n}\left[\frac{A_k}{j\omega-\lambda_k}+\frac{\bar{A}_k}{j\omega-\bar{\lambda}_k}+\frac{B_k}{-j\omega-\lambda_s}+\frac{\bar{B}_k}{-j\omega-\bar{\lambda}_s}\right] \tag{5}$$

where A_k is the k^{th} residue matrix of the PSD. As the output PSD itself the residue matrix is an $m\times m$ hermitian matrix and is given:

$$A_k = R_k C \sum_{k=1}^{n}\left[\frac{\bar{R}_s^T}{-\lambda_k-\bar{\lambda}_s}+\frac{R_s^T}{-\lambda_k-\lambda_s}\right] \tag{6}$$

The contribution to the residue from k^{th} mode is given by:

$$A_k = \frac{R_k C \bar{R}_k^T}{2\alpha_k} \tag{7}$$

where α_k is minus the real part of the pole $\lambda_k=-\alpha_k+j\omega_k$. As it appears, this term becomes dominating in case of light damping. It follows that the residue becomes proportional to the mode shape vector:

$$A_k = R_k C \bar{R}_k = \Phi_k \gamma_k^T C \gamma_k \Phi_k^T = d_k \Phi_k \Phi_k^T \tag{8}$$

where d_k is a constant scalar. At a certain frequency ω only a limited number of modes (typically one or two) will contribute significantly. Let Sub (ω) denote the number of these modes.

Therefore, in the case of a lightly damped structure, the response spectral density can always be written as:

$$G_{yy}(j\omega) = \sum_{k=Sub(\omega)}\frac{d_k \Phi_k \Phi_k^T}{j\omega-\lambda_k}+\frac{\bar{d}_k \bar{\Phi}_k \bar{\Phi}_k^T}{j\omega-\bar{\lambda}_k} \tag{9}$$

The EFDD technique uses the same technique as the FDD, but also computes the damping ratio. The response of the system can be expressed with the modal coordinates as follows (Brincker, *et al.* 2000):

$$\underline{y}(t) = \underline{\varphi}_1 q_1(t) + \underline{\varphi}_2 q_2(t) + ... = \underline{\underline{\Phi}}\,\underline{q}(t) \tag{10}$$

The correlation function is written as

$$\underline{\underline{C}}_y(\tau) = E\{\underline{y}(t+\tau)\underline{y}(t)^T\} \tag{11}$$

From Eq. (10), we can then write

$$\underline{\underline{C}}_y(\tau) = \{E\underline{y}(t+\tau)\underline{q}(t)^T\underline{\underline{\Phi}}^T\} = \underline{\underline{\Phi}}\,\underline{\underline{C}}_q(\tau)\,\underline{\underline{\Phi}}^T \tag{12}$$

The spectral response which depends on the frequency is written as follows:

$$\underline{\underline{S}}_y(f) = \underline{\underline{\Phi}}\,\underline{\underline{S}}_q(f)\,\underline{\underline{\Phi}}^T \tag{13}$$

The damping ratio ξ is defined as:

$$\xi \approx \frac{f_2 - f_1}{f_c} \tag{14}$$

where f_c is the frequency at the peaks of power spectral density and f_1 and f_2 are the frequencies corresponding to -3dB relative to the peak f_c.

4.4.3. EFDD Identification results

Fig. 11 shows the average of normalized singular values of spectral density matrices of all data sets using the EFDD technique. The singular values in this plot correspond to the detected frequencies. Table 3 shows the measurement-based estimates of the natural frequencies of the three detected vibration modes using the EFDD method. This table also shows the natural frequencies computed by

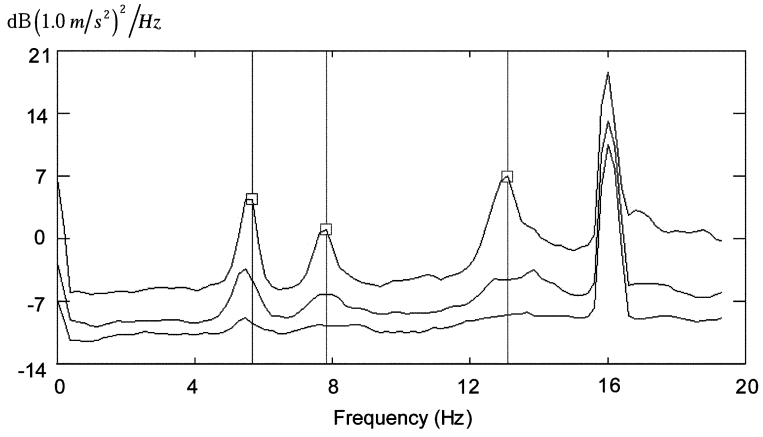

Fig. 11 Average of normalized singular values of spectral density matrices of all data sets using the EFDD technique

Table 3 Measurement-based estimates of the natural frequencies and damping ratios using the EFDD technique and computed frequencies before updating

Mode	Estimated from measurements using EFDD Technique		Computed frequency before updating (Hz)	Relative error between measured and computed frequency (%)
	Frequency (Hz)	Damping ratio (%)		
1	5.47	2.94	5.70	4.2
2	7.62	3.69	7.85	3.0
3	12.89	2.08	16.04	24.4

the program SAP2000 before updating and the relative error between these frequencies and the identified test frequencies. The error varies between 3% and 24%, indicating the need to update or correct the finite element model. This error could have been larger if the finite element model was less detailed, or the structure had not been adequately modelled. The measurement-based estimates of the damping ratios identified by the EFDD technique, shown in Table 2, range between 2.08% and 3.69% which are reasonable values for concrete structures. Figs. 12a, 12c and 12e show the measurement-based mode shapes identified using the EFDD algorithm for the three detected vibration modes. The first two modes are flexural modes while the third one is a torsional mode.

5. Finite element and model updating

5.1. Objective of finite element updating

The objective of finite element model updating is to obtain a reasonable correlation between experimental and numerical modal properties. The parameters selected for the updating were the concrete modulus of elasticity, the elastomeric bearing stiffnesses and the foundation spring stiffnesses. The updating consisted of performing a sensitivity analysis of the model stiffness matrix with respect to changes in these parameters. This translates to taking the derivative of the stiffness matrix with respect to these parameters.

The updating was performed based on two indicators that were applied simultaneously using the vertical displacement (z-direction): (a) comparison between computed and measured frequencies; and (b) comparison between computed and measured mode shapes. The comparison between the frequencies was estimated using the relative error between the computed and measured frequencies, while the comparison between the computed and measured mode shapes was evaluated using the MAC criterion (Allemang and Brown 2004). What follows is a review of the theory related to finite element updating.

5.2. Formulation of finite element updating

Finite element model updating is an iterative procedure performed using the program FEMTools (2004). The resulting matrix equation is of the form:

$$\{\Delta R\} = [S]\{\Delta P\} \tag{15}$$

where $\{\Delta P\}=\{P\}-\{P^0\}$ in which

- $\{P\}$ is a vector containing parameters from the numerical model. For the current case, these parameters are the Young's modulus of each element, the stiffness of the elastomeric bearings and the stiffness of the foundation springs.

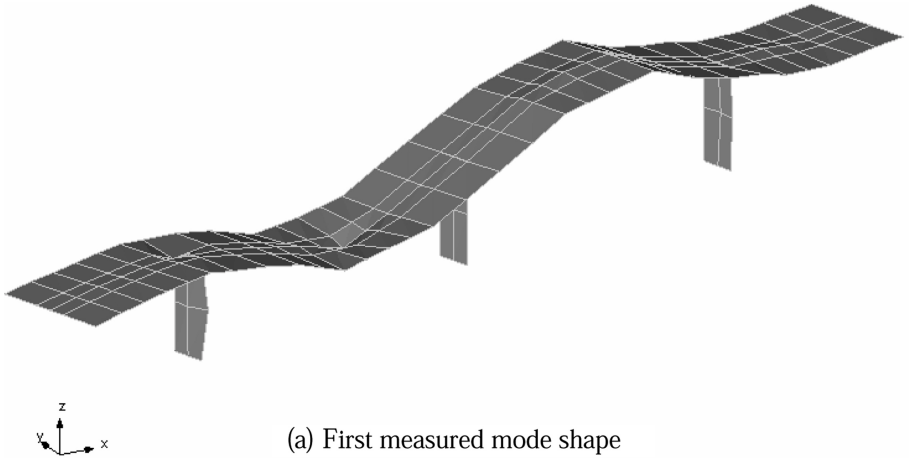

(a) First measured mode shape

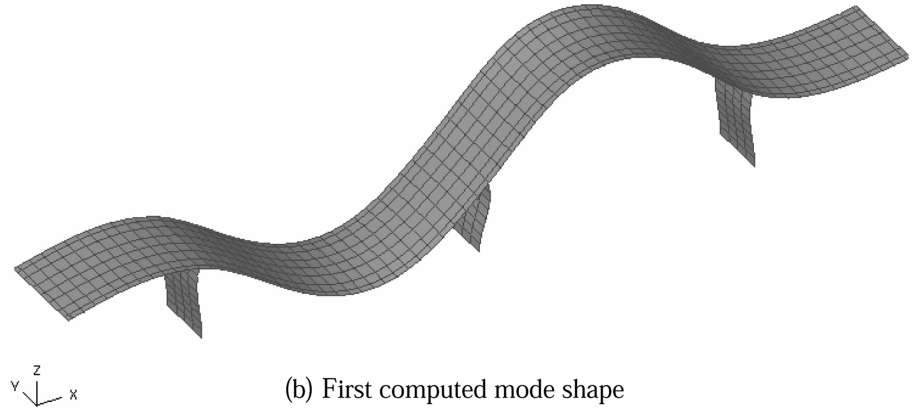

(b) First computed mode shape

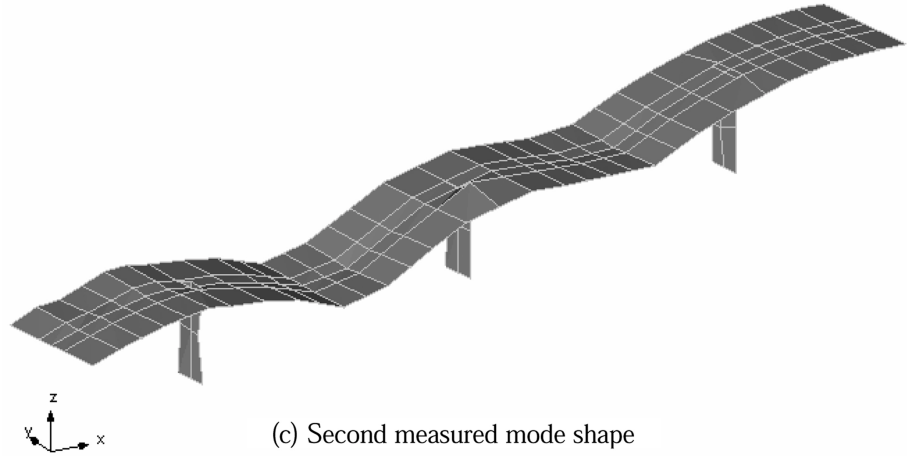

(c) Second measured mode shape

Fig. 12 Measurement-based mode shapes identified using the EFDD technique and computed mode shapes after updating

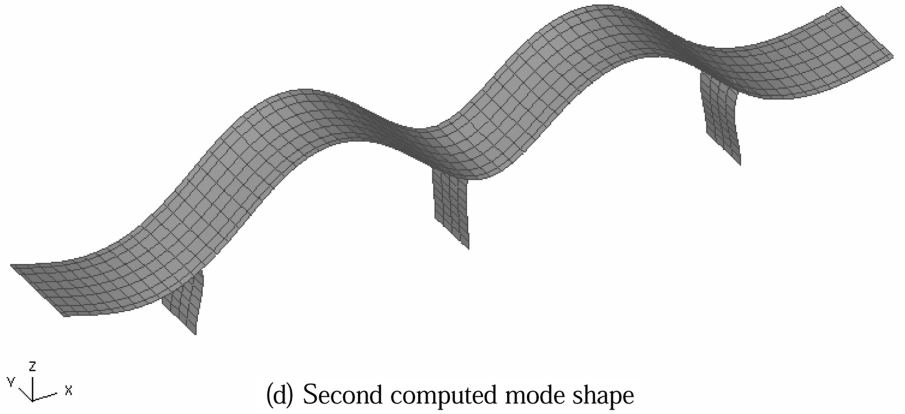

(d) Second computed mode shape

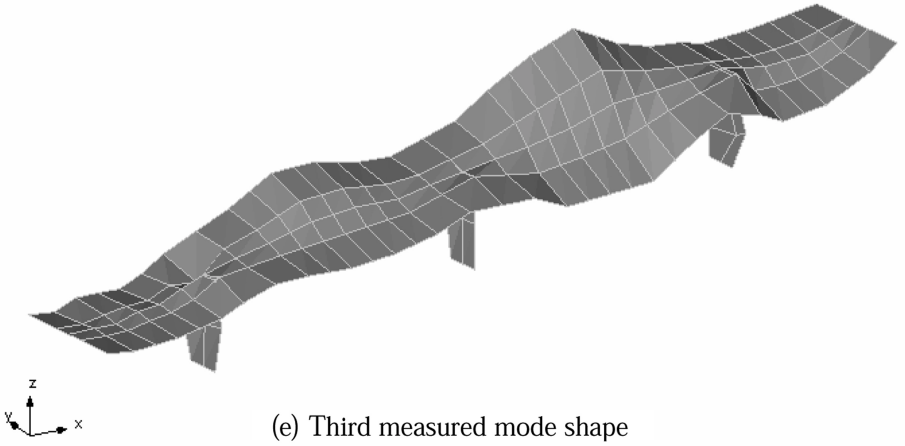

(e) Third measured mode shape

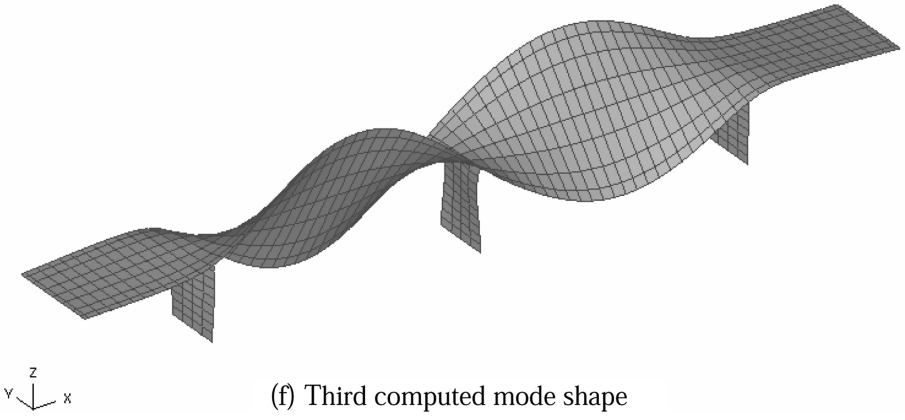

(f) Third computed mode shape

Fig. 12 Continued

- $\{P^0\}$ are the starting values of the parameters.

  and $\{\Delta R\}=\{R^e\}-\{R\}$ in which

- $\{R\}$ is a vector containing responses from the model. For the current case, they correspond to the numerical modes (frequencies) that are paired with the corresponding experimental ones and the numerical mode shapes.

• $\{R^e\}$ is the vector associated with the reference response test data.

The sensitivity matrix $[S]$ contains the gradients of the responses R with respect to parameters P.

$$[S] = S_{ij} = \frac{\partial R_i}{\partial P_j} \tag{16}$$

The updated values of parameters P are obtained from Eqs. (15) and (16):

$$\{P\} = \{P^0\} + [G](\{R^e\} - \{R\}) \tag{17}$$

where $[G]$ is the gain matrix computed following Bayesian estimation theory as:

$$[G] = [C_P][S]^T([C_R] + [S][C_P][S]^T)^{-1} \tag{18}$$

in which $[C_P]$ are weighting matrices that express the analyst's confidence in $\{P^0\}$ and the reference responses test data $\{R^e\}$.

Iterations are continued until error functions satisfy a convergence criterion.

5.3. Model updating results

Fig. 13 shows the normalized sensitivity for the 796 parameters which are: (a) 712 concrete elasticity moduli corresponding each to a shell element; (b) 13 elastomeric bearing stiffnesses and 15 foundation spring stiffnesses in the x-direction; (c) 13 elastomeric bearing stiffnesses and 15 foundation spring stiffnesses in the y-direction; (d) 13 elastomeric bearing stiffnesses and 15 foundation spring stiffnesses in the z-direction. It is clear from this figure that the dynamic response of the bridge is more sensitive to

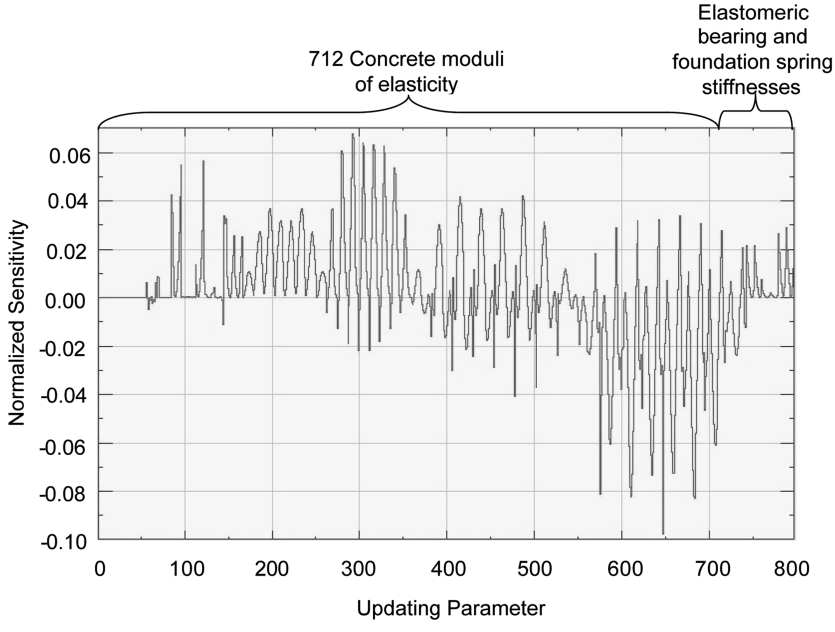

Fig. 13 Normalized sensitivity of selected parameters

Table 4 Measurement-based estimates of the natural frequencies using the EFDD technique and computed frequencies after updating

Mode	Measured frequency (Hz)	Computed frequency after updating (Hz)	Relative error between measured and computed frequency (%)	MAC between measured and computed mode shapes (%)
1	5.47	5.10	-6.8	97.9
2	7.62	7.19	-5.6	96.3
3	12.89	12.37	-4.0	81.3

Table 5 Percentage of number of elements in terms of changes in parameters selected for model updating

Modulus of elasticity (E)	
Parameter expressed in % of initial value	Ratio of number of elements to total number of elements (%)
100%	74.5
80% - 100%	3.4
60% - 80%	2.7
40% - 60%	2.8
20% - 40%	2.5
0% - 40%	14.0

Elastomeric Bearing Stiffness (Type A)				Elastomeric Bearing Stiffness (Type B)			
Parameter expressed in % of initial value	Kx_A	Ky_A	Kz_A	Parameter expressed in % of initial value	Kx_B	Ky_B	Kz_B
	Ratio of number of elements to total number of elements (%)				Ratio of number of elements to total number of elements (%)		
100%	0	100	25	100%	0	100	44.4
100%-150%	100	0	75	100%-150%	100	0	55.6

changes in the concrete modulus of elasticity.

Table 4 shows the test and model frequencies after updating obtained using 40 iterations. The relative error, which was before updating between 3% and 24% for the first three vibration modes (Table 3), became less than 6.8% as shown in Table 4. The measurement based mode shapes and computed updated mode shapes for the three detected modes are shown, respectively, in Figs. 12a, 12c, 12e and Figs. 12b, 12d, 12f. Table 4 also gives the MAC value between the updated Finite Element Mode Shapes and the Experimental Mode Shapes which is above 96% for the first two modes and 81% for the third mode. After updating, the error in the first two frequencies slightly increased at the expense of a relatively large reduction in the third frequency from about 24% to 4%. The small increase in the first two frequencies can be explained by the fact that the updating process was performed based on two indicators that were applied simultaneously, namely comparison of frequencies and comparison of mode shapes using the MAC criterion.

Table 5 gives the percentage of elements in terms of changes in parameters selected for model updating. This table indicates that 74.5% of the concrete elements remained intact while the rest of the elements suffered various degrees of reduction in the modulus of elasticity. Fig. 14 shows a contour plot of the concrete modulus of elasticity after updating. This figure indicates that most of the reduction in the concrete elasticity modulus took place in the center pier which, as mentioned in Section 4.2, was not

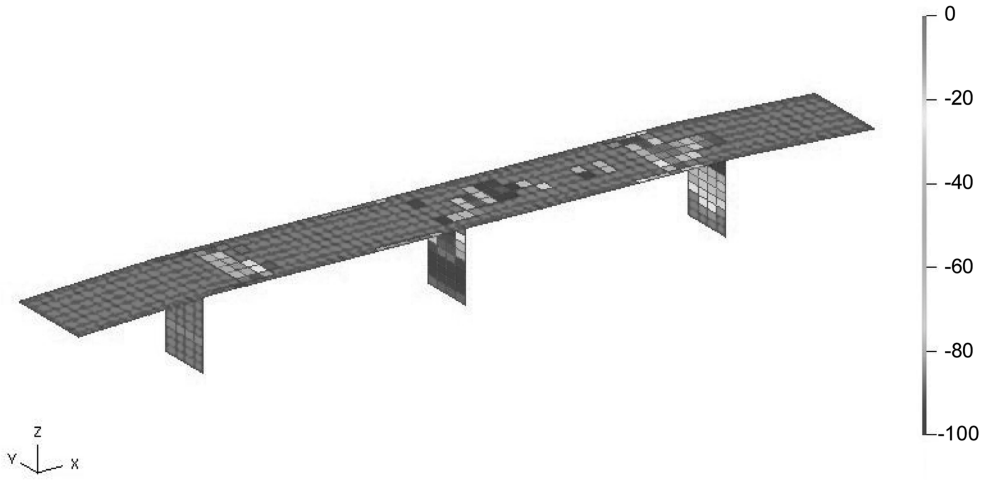

Fig. 14 Contour plot of the variations of concrete modulus of elasticity after updating

instrumented because its access was dangerous and the traffic along the highway could not be stopped to access this location. As a result, the value of 74.5% of the intact concrete elements may be interpreted as a possible underestimation indicating that the bridge has suffered relatively minor damage. Table 5 shows that 75% of the elastomeric bearing type A elements suffered an increase in stiffness in the *z*-direction compared to 55% for the case of the bearing type B elements. The foundation spring stiffnesses remained at the same order of magnitude of 10^{30} N/m indicating that the effect of the foundation on the dynamic behavior of the bridge was rather insignificant.

6. Conclusions

A rational methodology for the assessment of older reinforced concrete Tunisian bridges was applied on the Boujnah bridge as an alternative to a visual inspection methodology. This methodology is based on ambient vibration measurement of the bridge, identification of the structure's modal signature and finite element model updating. The modal properties for the first three vibration modes were successfully identified using the Enhanced Frequency Domain Decomposition technique.

The maximum error between the model and test frequencies before updating reached a value of 24% which indicated the need to update the finite element model. These errors became less than 6.8% after updating. Furthermore, a reasonable correlation between the experimental and finite element mode shapes was obtained at least for the first three vibration modes. The parameters selected for updating were the concrete modulus of elasticity, the elastomeric bearing stiffnesses and the foundation spring stiffnesses. The dynamic response of the bridge was shown to be more sensitive to changes in the concrete modulus of elasticity. Updating results revealed that the bridge has suffered relatively minor damage.

Acknowledgements

The authors are grateful for the funding provided by the Center for Testing and Construction

Techniques (CETEC) which is affiliated with the Tunisian Ministry of Infrastructure, Housing and Urban Planning. Sincere thanks are due to the technical and administrative personnel who assisted the authors in conducting the ambient vibration tests on the Boujnah bridge.

References

ARTeMIS Program Overview, http://www.svibs.com, accessed August 12th, 2004.

Allemang, R. J and Brown, D. L. (1982), "A correlation coefficient for modal vector analysis", *Proceedings of the 1st Int. Modal Analysis Conf. (IMAC)*, Orlando, Florida.

Brincker, R. and Andersen, P. (2000), "Ambient response analysis of the heritage court building structure", *Proceedings of the 18th Int. Modal Analysis Conf. (IMAC)*, San Antonio, Texas, 1081-1087.

Brincker, R., Andersen, P. and Frandsen, J. B. (2000), "Ambient response analysis of the great belt bridge", *Proceedings of the 18th Int. Modal Analysis Conf. (IMAC)*, San Antonio, Texas, 26-32.

Brincker, R., Andersen, P. and Zhang, L. (2000), "Modal identification from ambient responses using frequency domain decomposition", *Proceedings of the 18th Int. Modal Analysis Conf. (IMAC)*, San Antonio, Texas, 625-630.

CCBA (1968), Cahier des prescriptions communes, Règles techniques de conception et de calcul des ouvrages en béton armé, Fascicule 61, Titre VI, Bulletin officiel du Ministère de lequipement, du logement et du Ministère du Transport (in French).

Catbas, N., Ciloglu, K., Celebioglu, A., Popvics, J. and Aktan, E. (2001), *Proceedings of the 6th Annual Symp. on NDE for Health Monitoring and Diagnostics*, Newport Beach, California, USA, Fleet Health Monitoring of Large populations: Aged Concrete T-Beam Bridges in Pennsylvania.

Computers and Structures, Inc., 2000, SAP2000: Three Dimensional Static and Dynamic Finite Element Analysis and Design of Structures.

DasyLab Program Overview, http://www.dasylab.net/dasylab_english/, August 12th, (2004).

FEMTools Program Overview, http://www.femtools.com, August 12th, 2004.

Kinemetrics, Inc., (1997), *Operating Instructions for Vibration Survey System*, Model VSS-3000.

Kinemetrics, Inc., (2000), *Users Guide for the EpiSensor Force Balance Accelerometers, Model FBA ES-U*.

Phares, B. (2001), "Highlights of study of reliability of visual inspection", Presentation at the Annual Meeting of TRB Subcommittee A2C05(1) Non-destructive Evaluation of Structures, FHWA Report No. FHWA-RD-01-020 and FHWA-RD-01-021.

Van Overschee, P. and Moor, B. De. (1996), *Subspace Identification for Linear Systems: Theory, Implementations and Applications*. Kluwer Academic Publications.

CC